

Enhancement of electrocatalytic oxygen evolution by chiral molecular functionalization of hybrid 2D electrodes

Yunchang Liang, Karla Banjac, Kévin Martin, Nicolas Zigon, Seunghwa Lee, Nicolas Vanthuyne, Felipe Andrés Garcés-Pineda, José Galán-Mascarós, Xile Hu, Narcis Avarvari, et al.

▶ **To cite this version:**

Yunchang Liang, Karla Banjac, Kévin Martin, Nicolas Zigon, Seunghwa Lee, et al.. Enhancement of electrocatalytic oxygen evolution by chiral molecular functionalization of hybrid 2D electrodes. Nature Communications, 2022, 13 (1), pp.3356. 10.1038/s41467-022-31096-8 . hal-03855019

HAL Id: hal-03855019

https://univ-angers.hal.science/hal-03855019

Submitted on 16 Nov 2022

HAL is a multi-disciplinary open access archive for the deposit and dissemination of scientific research documents, whether they are published or not. The documents may come from teaching and research institutions in France or abroad, or from public or private research centers.

L'archive ouverte pluridisciplinaire **HAL**, est destinée au dépôt et à la diffusion de documents scientifiques de niveau recherche, publiés ou non, émanant des établissements d'enseignement et de recherche français ou étrangers, des laboratoires publics ou privés.

Enhancement of Electrocatalytic Oxygen Evolution by Chiral Molecular Functionalization of Hybrid 2D Electrodes

Yunchang Liang,[1,2,*] Karla Banjac,[1,2] Kévin Martin,[3] Nicolas Zigon,[3] Seunghwa Lee,[4] Nicolas Vanthuyne,[5] Felipe Andres Garcés-Pineda,[6] José R. Galan-Mascaros,[6,7] Xile Hu,[4] Narcis Avarvari,[3,*] Magalí Lingenfelder[1,2,*]

[1] Max Planck-EPFL Laboratory for Molecular Nanoscience and Technology, École Polytechnique Fédérale de Lausanne (EPFL), 1015 Lausanne, Switzerland

[2] Institut of Physics (IPHYS), Ecole Polytechnique Fédérale de Lausanne (EPFL), 1015 Lausanne, Switzerland

[3] Univ Angers, CNRS, MOLTECH-Anjou, SFR MATRIX, F-49000 Angers, France

[4] Laboratory of Inorganic Synthesis and Catalysis, Institute of Chemical Sciences and Engineering, École Polytechnique Fédérale de Lausanne (EPFL), 1015 Lausanne, Switzerland

[5] Aix Marseille Université, CNRS, Centrale Marseille, iSm2, Marseille, France

[6] Institute of Chemical Research of Catalonia (ICIQ), The Barcelona Institute of Science and Technology (BIST), Av. Països Catalans 16, E-43007 Tarragona, Spain

[7] Catalan Institution for Research and Advanced Studies (ICREA), Passeig Lluis Companys, 23, Barcelona 08010, Spain

*e-mail: yunchang.liang@epfl.ch; narcis.avarvari@univ-angers.fr; magali.lingenfelder@epfl.ch

Code de champ modifié

Code de champ modifié

Code de champ modifié

Abstract

A sustainable future requires highly efficient energy conversion and storage processes, where electrocatalysis plays a crucial role. The activity of an electrocatalyst is governed by the binding energy towards the reaction intermediates, while the scaling relationships prevent the improvement of a catalytic system over its volcano-plot limits. To overcome these limitations, unconventional methods that are not fully determined by the surface binding energy can be helpful. Here, we use organic chiral molecules, i.e., hetero-helicenes such as thiadiazole-[7]helicene and bis(thiadiazole)-[8]helicene, to boost the oxygen evolution reaction (OER) by up to ca. 130 % (at the potential of 1.65 V vs. RHE) at state-of-the-art 2D Ni- and NiFe-based catalysts *via* a spin-polarization mechanism. Our results show that chiral molecule-functionalization is able to increase the OER activity of catalysts beyond the volcano limits. A guideline for optimizing the catalytic activity *via* chiral molecular functionalization of hybrid 2D electrodes is given.

Main

Efficient electrocatalysis, especially electrocatalytic water-splitting, is imperative in future sustainable energy systems and carbon neutrality processes[1,2]. However, the complex reaction pathways and sluggish kinetics of the oxygen evolution reaction (OER) impede the application of electrocatalytic water-splitting[3]. The Sabatier principle states that an ideal catalyst surface should bind to the reaction intermediates with optimal strength (neither too weak nor too strong)[4]. Moreover, the binding energies of the variables of one adsorbate species to a catalyst surface follow a scaling relationship with each other. For instance, the adsorption free energies of OER reaction intermediates OH* and OOH* adhere to a simple relation, $\Delta G_{OOH^*} = \Delta G_{OH^*} + 3.2 \pm 0.2$ eV, for a large number of catalysts[5,6]. Consequently, a volcano-type plot confines the activity of the catalysts and guides the development of new catalytic surfaces[7,8,9]. Therefore, conventional strategies to enhance the catalytic activity are mostly based on adjusting the binding energy. Unconventional approaches, including magnetic control, can improve the electrocatalysis efficiency beyond the volcano limitations and are receiving increasing attention[10,11,12].

Electron transfer takes place during electrocatalysis processes. One of the inherent properties of electrons is the electron spin. Recently, it was reported that electron transport through a chiral molecule induces a spin polarization without external magnetic fields, i.e., after passing the molecule an imbalance between up and down spin is created[13,14,15,16]. This so-called chiral-induced spin selectivity (CISS) effect was suggested applicable in spin-dependent electron transfer processes at liquid/solid interfaces, for instance, the electrocatalytic OER[8,17]. It was suggested that the CISS process affects the spin of the electrons at the catalyst surface, consequently influencing the reaction pathway and enhancing the oxygen evolution. Therefore, it provides a unique opportunity to improve the activity and selectivity of the OER beyond the volcano plot-related restrictions.

However, experimentally decoupling the various coexisting effects contributing to OER is essential to assess the effect of chiral molecular functionalization. In particular, the high

dissolution rate of catalyst materials (e.g., Fe) under OER conditions[18], the weak bonding of thiol groups on metal oxides[19,20], the influence of organic molecules and their different structural conformers on the electrochemically active surface area (ECSA) and the coordination environment of the active surface sites[21] need to be considered. Therefore, well-defined systems are essential to decouple the effects of chiral molecular functionalization on the OER activity. Here, we use hybrid electrodes composed of a monolayer or sub-monolayer of rigid chiral/achiral molecules and 2D electrocatalysts in a sandwich configuration.

2D Ni (NiO_x) and NiFe ($NiFeO_x$) oxo-hydroxides are known as state-of-the-art electrocatalysts in alkaline media[22]. Carbohelicenes contain *ortho*-condensed aromatic rings with helical structures that possess axial chirality, and 2D self-assembly of helicene molecules on metals bestow chiral properties to the surface[23]. Their high racemization barriers[24] preserve their enantiopurity at the liquid/solid interface during the OER. The rigid structure of the helicenes also limits the number of molecular conformers at the electrode surface[25,26,27,28]. However, carbohelicenes interact weakly with metallic substrates (for instance, Cu, Ag, and Au) *via* van der Waals forces, resulting in high mobility of the molecules at room temperature[19,29]. Attachment of additional functional groups on helicenes is thus needed to increase the stability of such a hybrid electrode by strengthening the bonding to the metal surface[30]. Here, using chiral fused thiadiazole-helicene molecules, we report on the role of spin polarization by chiral molecular functionalization on the OER activity of metallic electrodes and the optimization of the chiral molecule-catalyst configuration for optimal activity.

Results and discussion

Effect of the molecular functionalization on the OER activity

In the first set of experiments, enantiopure (*M*)- and (*P*)-thiadiazole-[7]helicenes, previously reported by some of us[31] in the frame of our general interest in chiral molecular materials[32], have been used for the chiral molecular functionalization of metal electrodes.

Fig. 1 shows the effect of the adsorbed thiadiazole-[7]helicene enantiomers on the OER activity of two types of electrodes, namely Au(111) with monolayer NiO_x islands and bare Au(111), in O_2-saturated 0.1 M aqueous KOH solution. Farhat et al.[33] reported that the OER activity of ultrathin NiO_x and $NiFeO_x$ films under reaction conditions decreases over time in Fe-free KOH but stays more constant in unpurified (i.e., containing trace Fe impurities) KOH after Fe incorporation. Therefore, an unpurified KOH solution has been used to ensure all activity measurements are reproducible.

A clear enhancement in the OER current can be seen after the helicene molecules were deposited on NiO_x samples, as shown in **Fig. 1 a** and **b**. Deposition of (*P*)- and (*M*)-thiadiazole-[7]helicene enhances the OER current at 1.65 V vs. RHE approximately 85 % and 74 %, respectively. Electrochemical impedance spectroscopy (EIS) measurements were conducted before and after the molecule deposition to determine if the current enhancement could be just due to an increment in the ECSA during the molecule deposition process. The ECSA (proportional to the active surface) was obtained by determining the adsorption capacitance around the ‘‘onset’’ potential of the OER[34] (**Supplementary Figure 1 a)**. The OER currents normalized by the ECSA values still uphold the enhancement effect, i.e., ca. 61 % increase in the current density at 1.65 V vs. RHE and ca. 33.4 mV reduction in the overpotential at the current density of 10 mA cm^{-2} in the case of (*P*)-thiadiazole-[7]helicene (**Supplementary Figure 1 b**). It is likely that the increase in the adsorption capacitance in **Supplementary Figure 1 a** was mainly induced by the adsorbed helicene molecules[35,36], and not by the increment of the ECSA. A comparison of activity normalized by the EIS-determined ECSA and the Ni redox peaks is shown in **Supplementary Figure 1 c**. Nevertheless, the normalized current reinforces the conclusion that the thiadiazole-[7]helicene enantiomers are able to enhance the OER at NiO_x islands on Au surfaces.

Although the effectiveness of the helicene molecules on OER enhancement at NiO_x is validated, it is likely that molecules were not directly adsorbed on the NiO_x islands as no metallic Ni sites were accessible during the measurements. Direct thiadiazole bonding on metal oxide surfaces is difficult under the current conditions[37]. Therefore, the molecules were mostly adsorbed on the Au substrate. To test the effect of direct bonding between the helicene molecule and the catalyst surface on the OER, bare Au(111) electrodes were used for analogous OER experiments (**Fig. 1 c)**. Although such chirally functionalized Au(111) has lower OER activity compared to NiO_x, we anticipate that the activity measurements on Au(111) help to elucidate the effect of direct adsorption of helicene molecules at OER active sites. In contrast to the results from NiO_x samples, the presence of (*P*)-thiadiazole-[7]helicene molecules reduced the OER at the Au(111) surface. This difference can be ascribed to the different catalyst-helicene molecule configurations. At the NiO_x decorated Au substrates, the molecules were mostly adsorbed on the Au surfaces, and the active centers at NiO_x islands were not directly affected. At bare Au samples, the OER was taking place at the Au surface, which was partially blocked by the molecules after deposition. The exposed surface area of the Au samples was determined by the stripping of Pb atoms deposited by the underpotential deposition (UPD) method[38] (see **Supplementary Figure 4 a** and **b** for the Pb stripping results and the normalized current density). The results show that a submonolayer of helicene molecules was on the sample surface after the deposition. The decrease in the OER current is not proportional to the decrease in the surface area of Au. The helicene molecules even reduced the specific current density. As shown in **Supplementary Figure 4 a**, peak 1, which can be assigned to low-coordination and step sites[34,39], decreased and shifted towards more negative potentials. Zwaschka et al.[40] found that OER activity on a polycrystalline Au surface is dominated by < 1 % of the surface consisting of defects. Therefore, the molecules were more stably adsorbed on surface defects during the reactions.

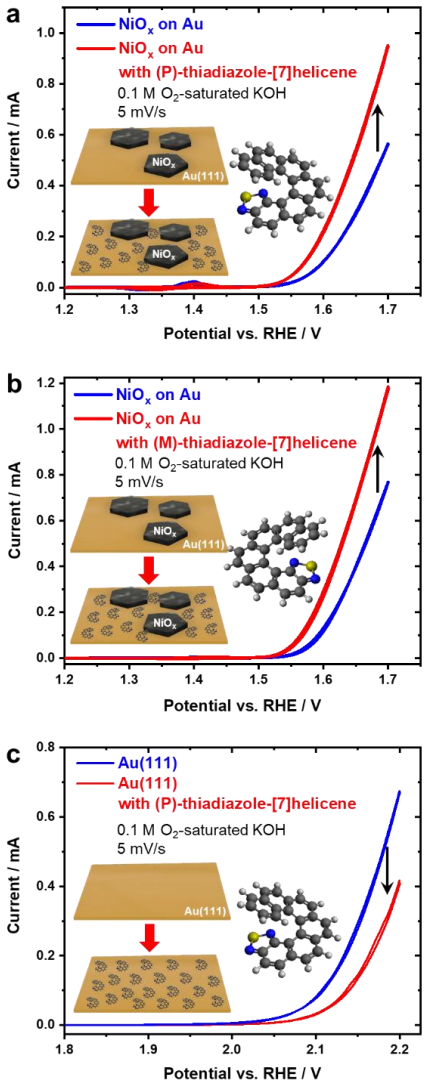


Fig. 1 | Helicene enantiomer functionalization effect on the OER activity. OER activity of **a** (*P*)-thiadiazole-[7]helicene and **b** (*M*)-thiadiazole-[7]helicene embedded NiO_x electrodes in 0.1 M O_2-saturated KOH.

Molecular functionalization vs. Fe doping effect on OER

Trotochaud et al. studied the effect of Fe impurities in the electrolyte and Fe doping in the catalysts on the OER activity, showing that Fe doping is efficient to improve the OER activity[41]. However, this improvement still adheres to the volcano-plot limits[42,43]. In this work, Fe impurities from the unpurified electrolyte had been incorporated in the NiO_x samples during activity measurements before chiral molecular functionalization. Additionally, we have also conducted OER activity measurements in Fe-free KOH. The Fe impurities in KOH were removed by the method described elsewhere[37]. Samples consisting of monolayer $NiFeO_x$ islands on Au surfaces were also used. A comparison of the activity enhancement caused by the (*P*)-thiadiazole-[7]helicene and the Fe doping in Ni-based catalysts is shown in **Fig. 2**. The Ni_9FeO_x catalyst shown in **Fig. 2 b** was deposited on a Ni foil using a combustion method introduced elsewhere[44]. The ECSA was obtained from the determination of the adsorption capacitance[30]. **Fig. 2 a** clearly shows that the helicene molecules increased the OER activity of Ni-based 2D islands modified by Fe doped directly in the catalysts or incorporated from the Fe-impurities-containing (unpurified) electrolyte. (*P*)-thiadiazole-[7]helicene reduces the overpotential at the current density of 1 mA cm^{-2} by approximately 0.025 V, 0.020 V and 0.023 V at NiO_x islands in Fe-free KOH, NiO_x islands in unpurified KOH and $NiFeO_x$ islands in unpurified KOH, respectively. The enhancement was higher on 2D $NiFeO_x$ islands deposited on a flat Au substrate than on Ni_9FeO_x deposited on a Ni foam, i.e., ca. 120 % and ca. 56 %, respectively, at the potential of 1.55 V vs. RHE. It is presumably caused by the different amounts of helicene molecules that can be embedded into different electrodes. On the Au substrates, helicene molecules were stably bonded to the Au surface. However, the Ni foam electrode surface only consists of metal oxides, which do not form strong interactions with the helicene molecules. The Ni foam electrodes have much higher roughness compared to the Au electrodes. The helicene molecules were probably inserted into the porous structures of the Ni foam. Nevertheless, the effect caused by the chiral molecules is independent and compatible with the Fe doping effect.

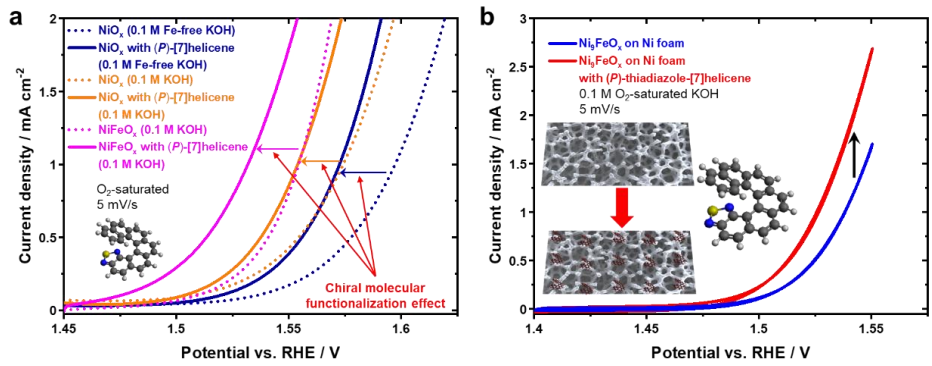


Fig. 2 | Comparison of chiral molecule effect with Fe-doping effect. a, chiral molecular functionalization enhancement on NiO_x islands in Fe-free, NiO_x islands in KOH (unpurified) and $NiFeO_x$ islands in KOH (unpurified). **b**, chiral molecular functionalization enhancement at Ni_9FeO_x deposited on Ni foam.

To confirm the enhancement is owing to the chirality of the adsorbed helicene molecules instead of other neglected properties of thiadiazole-[7]helicene and, at the same time, to investigate the influence of the helicene length on the OER, we synthesized bis(thiadiazole)-[8]helicene, which contains an additional thiadiazole ring at the opposite end of the helix, expected to stabilize the Au-helicene-NiO_x sandwich structure. We produced the racemic form of bis(thiadiazole)-[8]helicene and resolved the (*P*) and (*M*) enantiomers by chiral HPLC on Chiralpak IF (see **Methods** and the **Supplementary Information** for the synthesis, separation procedures and crystal structures). Suitable single crystals for the X-ray diffraction analysis have been obtained for both the enantiopure and also the racemic helicenes. The first eluted enantiomer was the dextrorotatory one, having a specific optical rotation of $[\alpha]_D^{25}$ = + (8100 ± 1 %)°, corresponding, as expected, to the clockwise (*P*) enantiomer, in agreement with the single crystal X-ray analysis. Mirror-image circular dichroism (CD) spectra were obtained for the two enantiomers (see **Supplementary Figure 17**). In the solid state, the helical curvature, characterizing the dihedral angle between the

two terminal thiadiazole rings, amounts at 29° for the racemate and 35° for the enantiopure compounds, thus smaller than 45° observed for the thiadiazole-[7]helicenes[27]. Then, with the new bis(thiadiazole)-[8]helicene in our hands, we set out to the chiral molecular functionalization of our electrodes.

Fig. 3 a shows that the activity of NiO_x on Au was improved by the presence of (*M*)-bis(thiadiazole)-[8]helicene molecules on the surface, with ca. 130 % enhancement at the potential of 1.65 V vs. RHE. A statistical analysis of enhancement at five nominally identical NiO_x electrodes can be seen in **Supplementary Figure 5**. The (*M*)-bis(thiadiazole)-[8]helicene yields a sensibly greater improvement in the OER current than the thiadiazole-[7]helicenes. The much more intense OER activity enhancement by the bis(thiadiazole)-[8]helicene functionalized electrodes compared to the thiadiazole-[7]helicene functionalized ones is in favor of this sandwich-type structure of the electrodes, with the helicene lying between the Au substrate and the NiO_x islands, since it can be hypothesized that the former strongly interacts with both the substrate and the catalyst thanks to the presence of the functional thiadiazole rings on both sides of the helical connector.

So far, the results show that chiral helicene molecules can enhance the OER activity. However, the compound in the molecules that directly bonds to the electrode surface is the thiadiazole group. Thus, it is essential to evaluate the role of thiadiazole. Accordingly, we used 2,1,3-benzothiadiazole, a simple achiral molecule containing a thiadiazole cycle fused to a benzene ring. It has the same molecular footprint bonds to the Au(111) surface as the helicene molecules used in this work. As shown in **Fig. 3 b**, the presence of the achiral molecules did not noticeably influence the OER activity of NiO_x islands on Au. Therefore, the interaction between the thiadiazole compound and the electrode surface is not the origin of the OER enhancement activity.

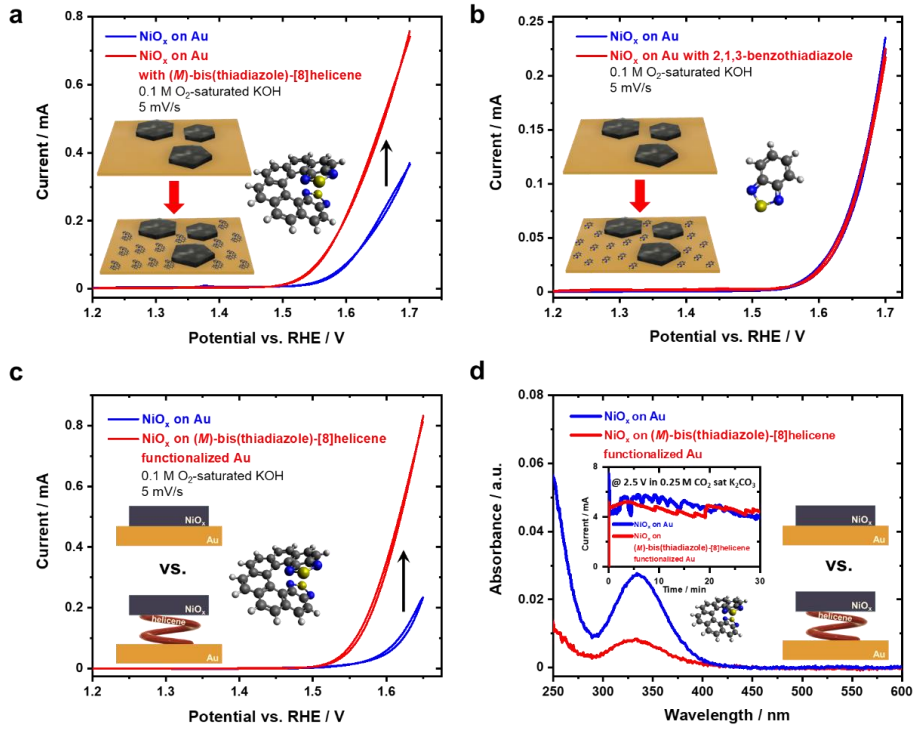


Fig. 3 | OER activity of NiO_x with chiral and achiral molecules and chiral molecular functionalization effect on the product selectivity. a,**b**, OER activity of **a** (*M*)-bis(thiadiazole)-[8]helicene on Au surface with NiO_x, **b** 2,1,3-benzothiadiazole on Au with NiO_x in 0.1 M O_2-saturated KOH. **c**, comparison of OER activity of NiO_x islands deposited on Au and NiO_x islands deposited on Au with a monolayer of (*M*)-bis(thiadiazole)-[8]helicene molecules. **d**, UV-visible spectrophotometry analysis of H_2O_2 production from chronoamperometry at 2.5 V vs. RHE (inset, see more details in **Supplementary Figure 6**) at NiO_x islands on Au and NiO_x islands on Au with a monolayer of (*M*)-bis(thiadiazole)-[8]helicene molecules. The absorbance spectra are normalized by the total charges transferred during the reaction.

To maximize the chiral molecular functionalization effect, we deposited the NiO_x islands on Au surface covered by a monolayer of (*M*)-bis(thiadiazole)-[8]helicene. The activity of this

sandwich configuration was compared to NiO_x islands (same NiO_x loading) directly deposited on Au surface without helicene molecules. The results are shown in **Fig. 3 c**. The enhancement in the current (ca. 250 % at 1.65 V vs. RHE without iR correction) is likely greater than the case where helicene molecules were added to the electrodes after NiO_x islands.

Water oxidation is a suitable example to test the chiral molecular functionalization effect on product selectivity, as H_2O_2 formation is expected to be reduced at spin-polarized surfaces[45]. However, NiO_x is not among the catalysts (e.g. ZnO, SnO_2 and TiO_2[46]) that selectively produce H_2O_2 during water oxidation. The OER at NiO_x based catalysts already dominates in alkaline media[47], and the production of H_2O_2 is neglectable in these conditions. ~~Moreover~~Moreover, ~~It~~ it is reported that a neutral solution containing bicarbonate enhances the faradaic efficiency towards H_2O_2 production[48,49], and the neutral pH also hinders the H_2O_2 from decomposition. ~~We~~ In order to test for changes in selectivity induced by the chiral molecules, we used the same electrode configurations in **Fig. 3 c** to confirm that the chiral molecular functionalization suppresses H_2O_2 production at neutral pH. ~~. Using the same catalyst materials prevents other unexpected influences, although NiO_x is not among the catalysts (e.g. ZnO, SnO_2 and TiO_2[50]) that selectively produce H_2O_2 during water oxidation.~~ Chronoamperometry (**Supplementary Figure 6**) and UV-visible spectrophotometry measurements (see **Methods**) were conducted in CO_2 saturated K_2CO_3 (neutral pH and containing a constant concentration of HCO_3^-). The H_2O_2 production was significantly reduced by the chiral molecular functionalization, as shown in **Fig. 3 d**. This is because H_2O_2 (a singlet species) formation is spin forbidden at a spin-polarized surface. This finding is in line with the CISS effect in water-splitting reported previously[13~~13~~,17~~17~~,45].

On Au(111) surfaces, the helicene molecules formed self-assembled monolayer (SAM) structures. The STM images of (*P*)-thiadiazole-[7]helicene and (*M*)-bis(thiadiazole)-[8]helicene molecules on Au(111) are shown in **Fig. 4 a** and **b**, respectively (see **Supplementary Figure 7** for larger scale images showing different domains of assemblies).

Commentaire [N1]: Add here re 47 which becomes 48

Commentaire [N2]: I would leav here only the ACS Appl. Energy Mater. (ref 48) since it's related t the bicarbonate influence, and would pass ref 47 (ACS Catal.) together with 49 (Nat. Commun.) since they both report different metal oxide catalysts (in 47 is about ZnO and I did not find any discussion related to bicarbonate

Commentaire [ML3]: agree

Commentaire [N4]: Add here re 47 which becomes 48

Mis en forme : Appel de note de fin, Non Exposant/ Indice

Mis en forme : Appel de note de fin, Non Exposant/ Indice

The former formed trimeric structures with approximately 0.75 molecules/nm^2, while the latter formed rows of dimers with approximately 1.1 molecules/nm^2. In the SAM of (*M*)-bis(thiadiazole)-[8]helicene molecules, the existence of three types of domains (60° to each other) is observed, as shown in **Supplementary Figure 7 b**. These types of molecular assemblies are common to other functionalized helicenes on Au(111)[21,22,23,25]. The molecular coverage of functionalized helicenes on the substrates determines the assembly, going from trimeric structures at low coverage to dimeric rows at high coverage[22,23,24,25]. Therefore, the (*M*)-bis(thiadiazole)-[8]helicene reached a higher coverage than the (*P*)-thiadiazole-[7]helicene under similar conditions, likely due to the added thiadiazole group.

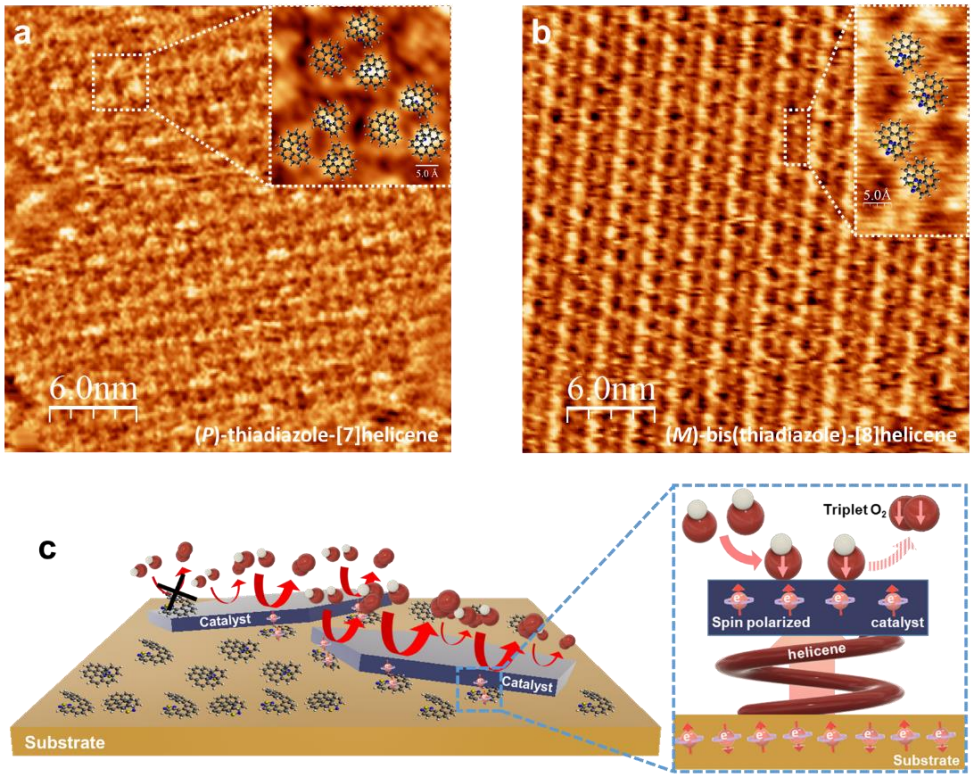


Fig. 4 | Helicene SAM and effect on the OER activity. a, an STM image of SAM of (*P*)-thiadiazole-[7]helicene (image size: 30 nm x 30 nm, tunneling current: 25 pA, sample bias: -5 mV). The dashed square marks a trimer of the molecules. A high resolution image (image size: 2.2 nm x 2.2 nm, tunneling current: 20 pA, sample bias: 20 mV) showing one trimer is

in the inset. **b**, an STM image of SAM of (*M*)-bis(thiadiazole)-[8]helicene on Au(111) (image size: 30 nm x 30 nm, tunneling current: 20 pA, sample bias: 25 mV). The dashed rectangle marks two dimers of the molecules. The inset shows a high resolution image (image size: 3 nm x 4 nm, tunneling current: 20 pA, sample bias: -25 mV) of two dimers. The 3D models of the molecules show the locations of the molecules. **c** Chiral molecule effect on the OER activity of NiO_x islands dependent on the catalyst- chiral molecule-Au substrate configuration and illustration of the chiral molecular spin polarization effect on the OER.

STM images were taken on the helicene molecule functionalized NiO_x samples after the OER measurements, as shown in **Supplementary Figure 8.** The NiO_x islands were roughened due to the OER, and the surfaces of the islands were likely not covered by the molecules. However, the structures on the Au surface suggest that the helicene molecule assembly on Au was stable during the OER. Bare Au surfaces can be seen in several areas in the images, which is in line with the Pb stripping measurement results in **Supplementary Figure 4**.

The activity enhancement using chiral molecules appears to depend on the anchoring of the molecules with regard to the catalysts. Based on our results, the dependence of the OER activity enhancement on the molecule-catalyst configuration is presented in **Fig. 4 c**. Helicene molecules on top of the catalyst surface block the active centers and consequently reduce the overall catalytic activity. Therefore, electrode manufacturing is vital to the performance of helicene molecule functionalized catalysts. A rationally designed electrode requires the catalytically active centers free of blockage and the electron transfer through the spin polarizers. For an optimal activity enhancement, the chiral molecules should be between the catalytic material and the substrate. A substrate that can strongly bond the chiral molecules (for example, Au in this work) is preferred for fabricating a stable electrode.

Chiral molecular functionalization

In this work, we show that chiral molecular functionalization can improve the OER activity of metal oxide catalysts. A specific catalyst-chiral helicene molecule-Au substrate configuration (as shown in **Fig. 4c**) shows the optimal catalytic activity. By comparing the effect of chiral helicene molecules and the achiral 2,1,3-benzothiadiazole, it is evident that such activity enhancement is directly related to the chirality of the molecules, rather than ligand effects introduced by the bonding of the molecules on the catalyst surface. The bonding between the catalyst and the chiral molecule alone does not cause any improvement in the catalytic activity. Contrarily, the bonding can reduce the activity when the chiral molecules are directly deposited at the catalyst active sites. The results of this comprehensive study are in agreement with the interpretation from Ref. 8 that a CISS-induced effect can efficiently enhance the OER.

In the CISS effect, the adsorption of chiral molecules on a surface spin-polarizes the interface[51,52,53]. In electron scattering, the spin polarization is induced by symmetry breaking[54]. This can be expanded to any process that can be described by a transition matrix, for example, photoemission, where the spin polarization is induced by the broken experimental symmetry also for light elements[55,56]. In electron transport, all contributions from the complex transition matrix elements are typically symmetric unless a chiral element is introduced. In this case, the transmitted electrons will acquire a spin polarization, similar to a paramagnetic material in an external magnetic field. Garcés-Pineda et al.[9] reported on the external magnetic field enhancement of the OER at various magnetic transition metal oxide-based catalysts. Although an activity enhancement can be caused by both chiral molecular functionalization and an external magnetic field, the enhancement magnitudes appear to be different. At the potential of 1.65 V vs. RHE, the OER current density (scan rate: 5 mV/s) on NiO_x-based catalysts in 0.1 M KOH increased ca. 61 % by using (*P*)-thiadiazole-[7]helicene, which is significantly larger than the ca. 10 % in 1 M KOH (scan rate: 5 mV/s) caused by an external magnetic field (≤450 mT)[9]. Thus, chiral molecular functionalization may be

comparatively more effective. It has also been well established that external magnetic fields can accelerate mass transfer processes through a magnetohydrodynamic effect [57,58,59]. The local magnetic field at the catalyst surface introduced by the chiral molecules and its effect on the local mass transfer should be further probed.

It was suggested that the electron spin at the catalyst surface strongly influences the bonding strength of the catalyst to oxygen species and the charge transfer between the catalyst and the oxygen adsorbates[9,60,61,62]. Electron spin polarization at catalyst surfaces with specifically modulated ferromagnetic properties leads to advanced OER kinetics[10,63,64,65], and a ferromagnetic catalyst can promote the spin polarization under an external magnetic field and thus enhances its OER activity[66]. However, not all practical OER catalysts are ferromagnetic. Additionally, metal oxide-based catalysts, especially highly active 2D nanostructured catalysts, undergo severe surface reconstruction processes under OER conditions[67,68,69]. The preservation of the well-prepared ferromagnetic properties under surface reconstruction is questionable. The chiral molecular functionalization provides a more versatile and sustainable electron spin polarization effect (**Fig. 4 c**). It can be applied to most catalysts independent of their electronic (magnetic) properties and under different reaction conditions, i.e., less affected by the catalyst composition and surface reconstruction.

Compared to chiral molecular functionalization, Fe doping is a verified way to improve the OER activity of Ni-based catalysts[70]. It is revealed that the OER activity of Ni-based catalysts in non-specifically treated electrolytes (containing a trace amount of Fe) is affected by the Fe doping, and the catalysts effectively turn into NiFe dual catalysts[37]. Our results show that chiral molecular functionalization enhancement can coexist with the Fe-doping effect and other alloying methods since the helicene molecules do not interact directly with the metal oxide active centers. Therefore, it is compatible with most metal oxide-based catalysis systems and independent of the chemical composition of the catalysts.

Moreover, the newly introduced (*M*)-bis(thiadiazole)-[8]helicene brings a higher enhancement to the OER than (*M*)-thiadiazole-[7]helicene, i.e., ca. 130 % vs. ca. 74 % in the

overall current at the potential of 1.65 V vs. RHE in 0.1 M KOH. This finding suggests the enhancement is related to the structure of the helicene molecules, for instance, molecular length and functional groups that determine the interactions with the catalyst and the substrates. Further enhancement through modification of the helicene molecules can be anticipated.

Conclusions

In summary, we have validated and evaluated the chiral molecular functionalization on the oxygen evolution at 2D hybrid chiral/achiral molecule-transition metal oxide electrodes. The results show that the chirality of the helicene molecules is accountable for a great enhancement in the activity of state-of-the-art OER catalysts. The enhancement is related to the electron spin polarization at the catalyst surface. However, the chiral molecular functionalization does not change the catalyst composition, and it is compatible with other enhancement methods, e.g., Fe doping. Therefore, this approach has the potential to boost electron spin-dependent catalytic reactions (e.g., the OER) beyond the common volcano-plot limits governed by the Sabatier principle and the scaling relationships. The comparison of different electrode configurations provides a clear guideline for optimizing the enhancement. This approach opens new avenues for developing next-generation catalytic systems with high efficiency and advanced selectivity through rational molecular functionalization.

Methods

Synthesis of (*rac*)-bis(thiadiazole)-[8]helicene. For the reaction Scheme, full experimental details, characterization, chiral HPLC separation and X-ray diffraction analysis details, see the **Supplementary Information**.

2,7-bis(benzothiadiazol)vinyl)naphthalene 2. 2,7-bis((triphenylphosphonium)methyl)naphthalene bromide **1** (0.26 g, 0.31 mmol, 1 equiv.) was suspended in 7 mL of dry THF under an argon atmosphere. The mixture was cooled down to -78°C and then *n*BuLi (0.41 mL, 1.6M in hexane, 0.65 mmol, 2.1 equiv.) was added dropwise. After 30 min at -78 °C, it was warmed to room temperature and stirred for one hour. The mixture was cooled down again to -78°C and benzothiadiazole-5-carbaldehyde was added (0.16 g, 0.097 mmol, 3.1 equiv.). The mixture was stirred 10 minutes at -78 °C, then warmed to room temperature and left at RT overnight. After filtration on Celite® and concentration under vacuum, column chromatography (SiO_2, petroleum ether: CH_2Cl_2 4 : 6) yielded **2** as a yellow powder (90 mg, 45% yield, mixture of Z/E isomers). ^{1}H NMR (300 MHz, $CDCl_3$): δ (ppm) 9.07z (s, 0.1H), 8.20-7.60 (m, 10H), 7.56-7.33 (m, 4H), 7.20-6.80 (m, 2H). δ (ppm) MS (MALDI) m/z = 448.0, theor. calc. 448.1($M^{\bullet+}$).

(*rac*)-bis(thiadiazole)-[8]helicene. 2,7-bis(benzothiadiazol)vinyl)naphthalene **2** (90 mg, 0.2 mmol, 1 equiv.) was dissolved in 350 mL of toluene in a photoreactor with a catalytic amount of iodine (ca. 0.1 equiv.) and the mixture was irradiated with an immersion lamp (150 W) for 20 hours. After evaporation of the solvent and column chromatography (SiO_2, PE : CH_2Cl_2 4:6) the compound was obtained as a yellow powder (40 mg, 44%). ^{1}H NMR (300 MHz, $CDCl_3$): δ (ppm) 8.17 (d, *J* = 8.2 Hz, 2H), 8.08 (s, 4H), 7.74 (d, *J* = 8.2 Hz, 2H), 7.51 (d, *J* = 9.2 Hz, 2H), 7.38 (d, *J* = 9.2 Hz, 2H). ^{13}C NMR (76 MHz, $CDCl_3$) δ (ppm) 153.76, 151.80, 133.25, 132.38, 132.18, 131.79, 129.81, 129.53, 128.54, 128.44, 127.84, 127.59, 126.17, 125.47, 123.66, 118.96. MS (MALDI) m/z = 444.0, theor. calc. 444.0 ($M^{\bullet+}$).

Sample preparation. Monolayer NiO_x and $NiFeO_x$ islands were synthesized by liquid exfoliation from the bulk counterparts reported elsewhere[71,72] and spin-coated on Au(111) film on mica substrates (epitaxial gold on mica, Georg Albert PVD – Beschichtungen). The

drop-casting method was used for the samples shown in **Fig. 3 c** and **d**, with 80 µL and 20 µL ink (1 mg NiO_x per 15 mL), respectively, to obtain the same catalyst loading for the comparisons of NiO_x on Au and the sandwich catalyst-molecule-Au configuration. Ni_9FeO_x on Ni foil electrodes were synthesized using a combustion method[40].

All molecules were first dissolved in dichloromethane (DCM, Sigma-Aldrich, puriss. p.a., ≥99.9% (GC)). The molecule solutions were drop-casted on the electrode surfaces to deposit a quasi-monolayer of molecules. After the DCM evaporated completely and all the molecules landed on the surfaces, the electrodes were rinsed with excessive DCM to remove molecules not adsorbed directly on the electrode surface. Afterwards, the electrodes were rinsed with Milli-Q water and ready for the OER activity measurement with adsorbed molecules.

The catalytic activity of Au surfaces is highly dependent on the surface morphology[73]. Under OER conditions, surface reconstruction continuously occurs on Au surfaces and strongly affects the OER activity[36]. Therefore, OER activity measurements of helicene molecule-functionalized Au surface used freshly prepared Au substrates (Au(111) film on mica substrates). Au samples for bare Au experiments were treated using pure DCM following the helicene deposition procedure; however, without helicene molecules dissolved in DCM. This treatment is to rule out the effect of the deposition procedure on other surface properties (e.g., roughness) that may influence the activity comparison. Identical experiments (activity and Pb stripping measurements) were conducted on bare Au and helicene molecule-functionalized Au.

Electrochemical characterization. The electrochemical measurements were conducted in a three-electrode cell. The overall activity depends on the absolute amount of catalysts deposited on the Au surface, which varies slightly between samples. An unpurified KOH solution (1N solution in water, ACROS Organics™) has been used in this work. The

measurements were kept running until stable CVs were observed. All electrochemical measurements were conducted using a VSP-300 (BioLogic) potentiostat. A coiled Au wire (99.9 %, Alfa Aesar) was used as the counter electrode (CE). The CE was cleaned by flame annealing and rinsed with Milli-Q (Millipore) water before each set of measurements. A HydroFlex® standard hydrogen reference electrode (Gaskatel) was used as the reference electrode (RE). The activity measurements were done without iR-correction to avoid overcompensation and only compare the effect of molecule deposition to the overall catalytic performance.

The effect of DCM washing on the OER activity is shown in **Supplementary Figure 3.** The activity was measured before and after washing the electrode with pure DCM. Afterwards, (*P*)-thiadiazole-[7]helicene molecules were deposited, and activity was measured again. The pure DCM washing had no noticeable effect on the activity, and enhancement can only be observed after (*P*)-thiadiazole-[7]helicene deposition. In this case, a Ag/AgCl (3 M NaCl) RE (BASi®) was used regarding the concern of using standard hydrogen reference electrodes for OER experiments in alkaline media from Garcia et al.[74]. The working electrode (WE) potential was converted to the RHE scale. Hence, the use of a Ag/AgCl RE likely leads to the same results as using the HydroFlex® standard hydrogen reference electrode in evaluating the chiral molecular functionalization effect. However, due to the lack of stability of the Ag/AgCl RE in long-term experiments[61], the HydroFlex® standard hydrogen reference electrode was used for the rest of the experiments reported in this work.

The EIS measurements were conducted as reported by Watzele et al.[30]. For NiO_x electrodes, the spectra were measured at the potential of 1.6 V vs. RHE (1.59 V vs. RHE in the case of $NiFeO_x$) close to the ‘‘onset’’ potential of the OER where reaction intermediates cover all active sites at NiO_x without interruptions from O_2 bubble formation. Each spectrum contains data at 198 frequencies from 30 kHz to 10 Hz measured using a probing signal amplitude of 10 mV, and the data fitting was done using EIS Data Analysis 1.3 software[75,76].

Chronoamperometry measurements were conducted in 0.25 M CO_2 saturated K_2CO_3 (prepared from Milli-Q water and Potassium carbonate powder, anhydrous, 99.99% trace metals basis, Sigma-Aldrich) to reduce the decomposition of H_2O_2. Each chronoamperometry measurement lasted 30 min at 2.5 V vs. RHE to have sufficient production of H_2O_2[48,49]. Afterwards, the electrolytes were taken into cleaned polypropylene centrifuge tubes and shaken well for H_2O_2 determination.

Commentaire [N5]: Be care if y update the refs

H_2O_2 determination. The H_2O_2 determination procedure was introduced by Fuku et al.[77]. 500uL of each electrolyte was added into 450 µL of 1 M HCl (prepared from Milli-Q water and hydrochloric acid semiconductor grade PURANAL™, fuming 37%, 37-38%, Sigma-Aldrich). Afterwards, 50 µL of 0.1 M $FeCl_2$ (from Iron(II) chloride tetrahydrate, puriss. p.a., ≥99.0% (RT), Sigma-Aldrich) in 1 M HCl was added. The well-mixed liquids were then taken to UV-visible spectrophotometry measurements using A Varian Cary 500 spectrophotometer. The peak around 335 nm appeared due to the change of Fe^{2+} to Fe^{3+} caused by the H_2O_2 in the electrolyte.

STM and AFM measurements. STM and AFM have been used to measure the deposition of the helicene molecules. A Bruker MS10 EC-STM with a NanoScope® V controller controlled by the software Nanoscope 8.15 has been used for the STM measurements. NCHR tips (NanoWorld®) were used for the AFM measurements in Tapping Mode with a Bruker Dimension FastScan AFM. Image analysis was done using the WSxM v5.0 Develop 9.1 software[78] and molecular scale models using LMAPper and Avogadro software. In the case of STM, nonanoic acid was added on the sample surface as the solvent for a solid/liquid interface to obtain a greater resolution than the one achieved at the solid/air interface[79,80].

Data availability

The data that support the findings of this study are available from the corresponding authors upon reasonable request.

References

[1] Roger, I., Shipman, M. A. & Symes, M. D. Earth-abundant catalysts for electrochemical and photoelectrochemical water splitting. *Nat. Rev. Chem.* **1,** 0003 (2017).

[2] Eisenberg, R., Gray, H. B. & Crabtree, G. W. Addressing the challenge of carbon-free energy. *Proc. Natl. Acad. Sci. USA* **117,** 12543–12549 (2020).

[3] Shiva Kumar, S. & Himabindu, V. Hydrogen production by PEM water electrolysis – A review. *Mater. Sci. Energy Technol.* **2,** 442–454 (2019).

[4] Che, M. Nobel Prize in chemistry 1912 to Sabatier: Organic chemistry or catalysis? *Catal. Today* **218,** 162–171 (2013).

[5] Christensen, R., Hansen, H. A., Dickens, C. F., Nørskov, J. K. & Vegge, T. Functional independent scaling relation for ORR/OER catalysts. *J. Phys. Chem. C* **120,** 24910–24916 (2016).

[6] Montoya, J., Seitz, L., Chakthranont, P. *et al.* Materials for solar fuels and chemicals. *Nat. Mater.* **16,** 70–81 (2017).

[7] Nørskov, J., Bligaard, T., Rossmeisl, J. et al. Towards the computational design of solid catalysts. *Nat. Chem.* **1,** 37–46 (2009).

[8] Medford, A. J. et al. From the Sabatier principle to a predictive theory of transition-metal heterogeneous catalysis. *J. Catal.* **328,** 36–42 (2015).

[9] Pérez-Ramírez, J. & López, N. Strategies to break linear scaling relationships. *Nat. Catal.* **2,** 971–976 (2019).

[10] Zhang, W., Banerjee-Ghosh, K., Tassinari, F. & Naaman, R. Enhanced Electrochemical Water Splitting with Chiral Molecule-Coated Fe_3O_4 Nanoparticles. *ACS Energy Lett.* **3,** 2308–2313 (2018).

[11] Garcés-Pineda, F. A., Blasco-Ahicart, M., Nieto-Castro, D., López, N. & Galán-Mascarós, J. R. Direct magnetic enhancement of electrocatalytic water oxidation in alkaline media. *Nat. Energy* **4,** 519–525 (2019).

[12] Li, X., Liu, H., Chen, Z. et al. Enhancing oxygen evolution efficiency of multiferroic oxides by spintronic and ferroelectric polarization regulation. *Nat. Commun.* **10,** 1409 (2019).

[13] Kiran, V. *et al*. Helicenes — a new class of organic spin filter. *Adv. Mater.* **28,** 1957–1962 (2016).

[14] Kettner, M. et al. Chirality-dependent electron spin filtering by molecular monolayers of helicenes. *J. Phys. Chem. Lett.* **9,** 2025–2030 (2018).

Mis en forme : Anglais (États Ur

Mis en forme : Français (France)

Mis en forme : Français (France)

[15] Naaman, R., Paltiel, Y. & Waldeck, D. H. Chiral molecules and the electron spin. *Nat. Rev. Chem.* **3,** 250–260 (2019).

[16] Brandt, J., Salerno, F. & Fuchter, M. The added value of small-molecule chirality in technological applications. *Nat. Rev. Chem.* **1,** 0045 (2017).

[17] Mtangi, W. et al. Control of Electrons' Spin Eliminates Hydrogen Peroxide Formation During Water Splitting. *J. Am. Chem. Soc.* **139,** 2794–2798 (2017).

[18] Chung, D. Y. et al. Dynamic stability of active sites in hydr(oxy)oxides for the oxygen evolution reaction. *Nat. Energy* **5,** 222–230 (2020).

[19] Love, J. C., Estroff, L. A., Kriebel, J. K., Nuzzo, R. G. & Whitesides, G. M. Self-Assembled Monolayers of Thiolates on Metals as a Form of Nanotechnology. *Chem. Rev.* **105,** 1103–1170 (2005).

[20] Grimm, O. C., Somaratne, R. M. D. S., Wang, Y., Kim, S. & Whitten, J. E. Thiol adsorption on metal oxide nanoparticles. *Phys. Chem. Chem. Phys.* **23,** 8309–8317 (2021).

[21] Miner, E. M. & Dincă, M. Metal-organic frameworks: Evolved oxygen evolution catalysts. *Nat. Energy* **1,** 16186 (2016).

[22] Song, F., Hu, X. Exfoliation of layered double hydroxides for enhanced oxygen evolution catalysis. *Nat. Commun.* **5,** 4477 (2014).

[23] Ernst, K.-H. Stereochemical Recognition of Helicenes on Metal Surfaces. *Acc. Chem. Res.* **49,** 1182–1190 (2016).

[24] Barroso, J. et al. Revisiting the racemization mechanism of helicenes. *Chem. Commun.* **54,** 188–191 (2018).

[25] Balandina, T. et al. Self-assembly of an asymmetrically functionalized [6]helicene at liquid/solid interfaces. *Chem. Commun.* **49,** 2207 (2013).

[26] Ascolani, H. et al. Van der Waals interactions in the self-assembly of 5-amino [6]helicene on Cu(100) and Au(111). *Chem. Commun.* **50,** 13907–13909 (2014).

[27] van der Meijden, M. W. et al. Synthesis, Properties, and Two-Dimensional Adsorption Characteristics of [6]Hexahelicene-7-carboxylic acid. *Chem. Eur. J.* **22,** 14633–14639 (2016).

[28] Fuhr, J. D. et al. Chiral expression of adsorbed (MP) 5-amino[6]helicenes: from random structures to dense racemic crystals by surface alloying. *Chem. Commun.* **53,** 130–133 (2017).

Mis en forme : Français (France)

[29] Seibel, J., Parschau, M. & Ernst, K.-H. Two-Dimensional Crystallization of Enantiopure and Racemic Heptahelicene on Ag(111) and Au(111). *J. Phys. Chem. C* **118,** 29135–29141 (2014).

[30] Krukowski, P. et al. Adsorption and Light Emission of a Racemic Mixture of [7]thiaheterohelicene-2,13-carboxaldehyde on Au(111), Cu(001), and NiAl(110) Surfaces Investigated Using a Scanning Tunneling Microscope. *J. Phys. Chem. C* **125,** 9419–9427 (2021).

[31] Biet, T. et al. Triggering Emission with the Helical Turn in Thiadiazole-Helicenes. *Chem. Eur. J.* **23,** 437–446 (2017).

[32] Pop, F., Zigon, N. & Avarvari, N. Main-Group-Based Electro- and Photoactive Chiral Materials. *Chem. Rev.* **119,** 8435–8478 (2019).

[33] Farhat, R., Dhainy, J. & Halaoui, L. I. OER Catalysis at Activated and Codeposited NiFe-Oxo/Hydroxide Thin Films Is Due to Postdeposition Surface-Fe and Is Not Sustainable without Fe in Solution. *ACS Catal.* **10,** 20–35 (2020).

[34] Watzele, S. et al. Determination of Electroactive Surface Area of Ni-, Co-, Fe-, and Ir-Based Oxide Electrocatalysts. *ACS Catal.* **9,** 9222–9230 (2019).

[35] Tounsi, M. et al. Electrochemical Capacitive K^+ EMIS Chemical Sensor Based on the Dibromoaza[7]helicene as an Ionophore for Potassium Ions Detection. *Electroanalysis* **28,** 2892–2899 (2016).

[36] Tounsi, M. et al. A novel EIS field effect structures coated with TESUD-PPy-PVC-dibromoaza[7]helicene matrix for potassium ions detection. *Mater. Sci. Eng. C* **61,** 608–615 (2016).

[37] Sadler, J. E. et al. Surface functionalization of electro-deposited nickel. *Phys. Chem. Chem. Phys.* **13,** 17987 (2011).

[38] Mitchell, C., Fayette, M. & Dimitrov, N. Homo- and hetero-epitaxial deposition of Au by surface limited redox replacement of Pb underpotentially deposited layer in one-cell configuration. *Electrochim. Acta* **85,** 450–458 (2012).

[39] Jeyabharathi, C., Zander, M. & Scholz, F. Underpotential deposition of lead on quasi-spherical and faceted gold nanoparticles. *J. Electroanal. Chem.* **819,** 159–162 (2018).

[40] Zwaschka, G. et al. Imaging the Heterogeneity of the Oxygen Evolution Reaction on Gold Electrodes Operando: Activity is Highly Local. *ACS Catal.* **10,** 6084–6093 (2020).

Mis en forme : Français (France)

[41] Trotochaud, L., Young, S. L., Ranney, J. K. & Boettcher, S. W. Nickel–Iron Oxyhydroxide Oxygen-Evolution Electrocatalysts: The Role of Intentional and Incidental Iron Incorporation. *J. Am. Chem. Soc.* **136,** 6744–6753 (2014).

[42] Dionigi, F. & Strasser, P. NiFe-Based (Oxy)hydroxide Catalysts for Oxygen Evolution Reaction in Non-Acidic Electrolytes. *Adv. Energy Mater.* **6,** 1600621 (2016).

[43] Song, F. et al. An Unconventional Iron Nickel Catalyst for the Oxygen Evolution Reaction. *ACS Cent. Sci.* **5,** 558–568 (2019).

[44] Garces-Pineda, F. A. et al. Push-pull electronic effects in Surface-active sites enhance electrocatalytic oxygen evolution on transition metal oxides. *ChemSusChem* **14,** 1595–1601 (2021)

[45] Mtangi, W., Kiran, V., Fontanesi, C. & Naaman, R. The role of the electron spin polarization in water splitting. *J. Phys. Chem. Lett.* **6,** 4916–4922 (2015).

[46] Shi, X., Siahrostami, S., Li, GL. *et al.* Understanding activity trends in electrochemical water oxidation to form hydrogen peroxide. *Nat. Commun.* **8,** 701 (2017).

[47] Görlin, M. et al. Tracking catalyst redox states and reaction dynamics in Ni–Fe oxyhydroxide oxygen evolution reaction electrocatalysts: the role of catalyst support and electrolyte pH. *J. Am. Chem. Soc.* **139**, 2070–2082 (2017).

[48] Kelly, S. et al. ZnO as an active and selective catalyst for electrochemical water oxidation to hydrogen peroxide. *ACS Catal.* **9**, 4593–4599 (2019).

[49] Gill, T. M., Vallez, L. & Zheng, X. Enhancing Electrochemical Water Oxidation toward H_2O_2 via Carbonaceous Electrolyte Engineering. *ACS Appl.ied Energy Mater.ials* **4**, 12429–12435 (2021).

[50] ~~Shi, X., Siahrostami, S., Li, GL. *et al.* Understanding activity trends in electrochemical water oxidation to form hydrogen peroxide. *Nat. Commun.* **8,** 701 (2017).~~

[51] Ghosh, S. et al. Effect of chiral molecules on the electron's spin wavefunction at interfaces. *J. Phys. Chem. Lett.* **11,** 1550–1557 (2020).

[52] Naaman, R., Paltiel, Y. & Waldeck, D. H. Chiral molecules and the spin selectivity effect. *J. Phys. Chem. Lett.* **9,** 3660–3666 (2020).

[53] Mishra, S. et al. Length-dependent electron spin polarization in oligopeptides and DNA. *J. Phys. Chem. C* **124,** 10776–10782 (2020).

[54] Kessler, J. *Polarized Electrons* (Springer, 1985).

Mis en forme : Anglais (États Un

Mis en forme : Français (France)

Mis en forme : Français (France)

[55] Heinzmann, U. & Dil, J. H. Spin–orbit-induced photoelectron spin polarization in angle-resolved photoemission from both atomic and condensed matter targets. *J. Phys. Condens. Matter* **24,** 173001 (2012).

[56] M. Fanciulli et al., Spin Polarization and Attosecond Time Delay in Photoemission from Spin Degenerate States of Solids. *Phys. Rev. Lett.* **118,** 067402 (2017).

[57] Li, Y., Zhang, L., Peng, J., Zhang, W. & Peng, K. Magnetic field enhancing electrocatalysis of Co_3O_4/NF for oxygen evolution reaction. *J. Power Sources* **433,** 226704 (2019).

[58] L. M. A. Monzon, J. M. D. Coey, Magnetic fields in electrochemistry: The Lorentz force. A mini-review. *Electrochem. Commun.* **42,** 38–41 (2014).

[59] V. Gatard, J. Deseure, M. Chatenet. Use of magnetic fields in electrochemistry: a selected review. *Curr. Opin. Electrochem*. **23,** 96-105 (2020).

[60] Suntivich, J., May, K. J., Gasteiger, H. A., Goodenough, J. B. & Shao-Horn, Y. A perovskite oxide optimized for oxygen evolution catalysis from molecular orbital principles. *Science* **334,** 1383–1385 (2011).

[61] Gracia, J. Spin dependent interactions catalyse the oxygen electrochemistry. *Phys. Chem. Chem. Phys.* **19,** 20451–20456 (2017).

[62] Gracia, J. Itinerant spins and bond lengths in oxide electrocatalysts for oxygen evolution and reduction reactions. *J. Phys. Chem. C* **123,** 9967–9972 (2019).

[63] Chen, R. R. et al. Antiferromagnetic inverse spinel oxide $LiCoVO_4$ with spin-polarized channels for water oxidation. *Adv. Mater.* **32,** 1907976 (2020).

[64] Sun, Y. et al. Spin-related electron transfer and orbital interactions in oxygen electrocatalysis. *Adv. Mater.* **32,** 2003297 (2020).

[65] Wu, T., Ren, X., Sun, Y. et al. Spin pinning effect to reconstructed oxyhydroxide layer on ferromagnetic oxides for enhanced water oxidation. *Nat. Commun.* **12,** 3634 (2021).

[66] Ren, X., Wu, T., Sun, Y. et al. Spin-polarized oxygen evolution reaction under magnetic field. *Nat. Commun.* **12,** 2608 (2021).

[67] Deng, J. et al. Morphology dynamics of single-layered $Ni(OH)_2$/NiOOH nanosheets and subsequent Fe incorporation studied by in situ electrochemical atomic force microscopy. *Nano Lett.* **17,** 6922–6926 (2017).

Mis en forme : Français (France)

Mis en forme : Français (France)

Mis en forme : Français (France)

[68] Dette, C., Hurst, M. R., Deng, J., Nellist, M. R. & Boettcher, S. W. Structural evolution of metal (oxy)hydroxide nanosheets during the oxygen evolution reaction. *ACS Appl. Mater. Interfaces* **11,** 5590–5594 (2019).

[69] Gao, L., Cui, X., Sewell, C. D., Li, J. & Lin, Z, Recent advances in activating surface reconstruction for the high-efficiency oxygen evolution reaction. *Chem. Soc. Rev.* **50,** 8428–8469 (2021).

[70] Anantharaj, S., Kundu, S. & Noda, S. "The Fe Effect": A review unveiling the critical roles of Fe in enhancing OER activity of Ni and Co based catalysts. *Nano Energy* **80,** 105514 (2021).

[71] Ida, S., Shiga, D., Koinuma, M. & Matasumto, Y. Synthesis of hexagonal nickel hydroxide nanosheets by exfoliation of layered nickel hydroxide intercalated with dodecyl sulfate ions. *J. Am. Chem. Soc.* **130,** 14038–14039 (2008).

[72] Song, F. & Hu, X. Exfoliation of layered double hydroxides for enhanced oxygen evolution catalysis. *Nat. Commun.* **5,** 4477 (2014).

[73] Liu, L. & Corma, A. Metal catalysts for heterogeneous catalysis: from single atoms to nanoclusters and nanoparticles. *Chem. Rev.* **118,** 4981–5079 (2018).

[74] Garcia, A. C. & Koper, M. T. Effect of Saturating the Electrolyte with Oxygen on the Activity for the Oxygen Evolution Reaction. *ACS Catal.* **8,** 9359-9363 (2018).

[75] Kanoun O Lecture notes on impedance spectroscopy: measurement, modelling and applications. CRC Press, Boca Raton, p 112. (2011).

[76] A.S. Bondarenko, Analysis of large experimental datasets in electrochemical impedance spectroscopy, *Anal. Chim. Acta* **743,** 41–502012 (2012).

[77] Fuku, K., Miyase, Y., Miseki, Y., Gunji, T. & Sayama, K. Enhanced oxidative hydrogen peroxide production on conducting glass anodes modified with metal oxides. *ChemistrySelect* **1,** 5721–5726 (2016).

[78] Horcas, I. et al. WSXM: A software for scanning probe microscopy and a tool for nanotechnology. *Rev. Sci. Instrum.* **78,** 013705 (2007).

[79] Cometto, F. et al. The STM bias voltage-dependent polymorphism of a binary supramolecular network. *Chem. Commun.* **53,** 11430–11432 (2017).

[80] Ubink, J., Enache, M. & Stöhr, M. Bias-induced conformational switching of supramolecular networks of trimesic acid at the solid-liquid interface. *J. Chem. Phys.* **148,** 174703 (2018).

Acknowledgements

We heartily thank Prof. Hugo Dil for sharing his input on the discussion of the CISS effect in terms of spin polarization. S.L. acknowledges financial support by the Marie Skłodowska-Curie Fellowship (No. 838367 to S.L.) under the European Union's Horizon 2020 research. K.M., N.Z., N.V. and N.A. acknowledge the support from the CNRS, the University of Angers and the RFI LUMOMAT (grant to K.M.) in France. M.L. and N.A. thank the Swiss Academies of Arts and Sciences (SATW) and the French Ministry of Foreign Affairs for financial support through the bilateral Germaine de Staël (PHC Project 47931VB) project. J.R.G.M. and F.A.G.P. thank the financial support of the FEDER/Ministerio de Ciencia e Innovación, Agencia Estatal de Investigación (RTI2018-095618-B-I00); the Generalitat de Catalunya (2017-SGR-1406), the CERCA Programme/Generalitat de Catalunya.

Author contributions

Y.L., K.B., N.A, and M.L. conceived and designed the experiments. N.A. and M.L. supervised the project and led the collaboration efforts. Y.L., K.B carried out the scanning probe and electrochemical measurements. K.M., N.Z., and N.V. synthesized the helicenes and performed the enantiomer resolution. S.L., F.A.G.P., J.R.G.M., synthesized the catalysts. All authors participated in the result discussions. The manuscript was written by Y.L., N.A., and M.L. with contributions from all the authors.